ACS APPLIED MATERIALS & INTERFACES

Research Article

www.acsami.org

Comparative Study on Pyrido[3,4-*b*]pyrazine-Based Sensitizers by Tuning Bulky Donors for Dye-Sensitized Solar Cells

Xiaoyu Zhang,[†] Jiangyi Mao,[†] Dan Wang,[†] Xin Li,*[,‡] Jiabao Yang,[†] Zhongjin Shen,[†] Wenjun Wu,[†] Jing Li,*[,†] Hans Ågren,[‡] and Jianli Hua*[,†]

[†]Key Laboratory for Advanced Materials and Institute of Fine Chemicals, East China University of Science and Technology, Shanghai 200237, People's Republic of China

[‡]Division of Theoretical Chemistry and Biology, School of Biotechnology, KTH Royal Institute of Technology, SE-10691 Stockholm, Sweden

Supporting Information

ABSTRACT: Dye-sensitized solar cells (DSSCs) with cobalt electrolytes have gained increasing attention. In this Research Article, two new pyrido[3,4-*b*]-pyrazine-based sensitizers with different cores of bulky donors (indoline for **DT-1** and triphenylamine for **DT-2**) were designed and synthesized for a comparative study of their photophysical and electrochemical properties and device performance and were also analyzed through density functional theory calculations. The results of density function theory calculations reveal the limited electronic communication between the biphenyl branch at the cis-position of *N*-phenylindoline and the indoline core, which could act as an insulating blocking group and inhibit the dye aggregation and charge recombination at the interface of TiO_2/dye/electrolyte. As expected, DSSCs based on **DT-1** with cobalt redox electrolyte gained a higher photoelectric conversion efficiency of 8.57% under standard AM 1.5 G simulated sunlight, with J_{sc} = 16.08 mA cm^{-2}, V_{oc} = 802 mV, and FF = 0.66. Both electrochemical impedance spectroscopy (EIS) and intensity-modulated photovoltage spectroscopy (IMVS) suggest that charge recombination in DSSCs based on **DT-1** is much less than that in their counterparts of **DT-2**, owing to the bigger donor size and the insulating blocking branch in the donor of **DT-1**.

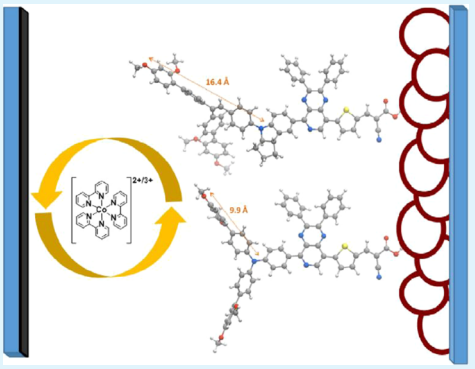

KEYWORDS: *sensitizers, pyrido[3,4-b]pyrazine, indoline, triphenylamine, dye-sensitized solar cells*

INTRODUCTION

As a promising technology for the new generation of photovoltaic systems, dye-sensitized solar cells (DSSCs) have attracted tremendous attention due to their ecological and economical fabrication processes since the first report in 1991.[1−7] Each component of the DSSC (i.e., sensitizer, electrolyte, photoanode, and counter electrode) plays an important role in the photovoltaic performance. As one of the key components, the redox electrolyte has been demonstrated to be very crucial in determining the photoelectric conversion efficiency and device stability of DSSCs.[8,9] So far, the most commonly used redox mediator is iodide/triiodide (I^-/I_3^-), which has showed remarkable performance in DSSCs owing to its desirable kinetic properties and high carrier collection efficiencies.[10,11] However, the I_3^-/I^- redox couple suffers from several intrinsic disadvantages including a low redox potential (~0.4 V vs NHE), competitive blue light absorption and corrosion toward metal materials, which pose a negative influence on the open-circuit voltage (V_{oc}), the short-circuit current density (J_{sc}), the device stability, and in turn the solar-to-electric power conversion efficiency (η) as well as the scaled-up applications of DSSCs.[9,12] In order to improve the situation, more researches have been focused on finding alternative redox electrolytes with the main goal of increasing the V_{oc} in the past decade.[13−18] Among the candidate redox electrolytes, cobalt (II/III) tris-bipyridyl redox shuttle became popular due to its tunable redox potential, negligible light absorption and remarkable performance.[19−22] The state-of-the-art DSSCs based on zinc porphyrin complexes with cobalt electrolyte have achieved an amazing η of over 12%.[23,24] However, compared to the I_3^-/I^- redox shuttle, the larger size, heavier mass and lower diffusion coefficient of the cobalt complex lead to mass transport and charge recombination problems, which limits the thickness of TiO_2 films, and hence the light-harvesting abilities of the cell devices.[25,26] Therefore, metal-free organic sensitizers have been becoming increasingly attractive owing to their high extinction coefficients, versatility of molecular structure, tunable energy levels and absorptivity.[27−30] What's more, the recombination can be reduced by tuning the molecular structure.

Earlier research on DSSCs based on organic sensitizers with cobalt electrolytes have indicated that these suffer from severe

Received: November 11, 2014
Accepted: January 12, 2015
Published: January 12, 2015

DOI: 10.1021/am507824h
ACS Appl. Mater. Interfaces 2015, 7, 2760−2771

Scheme 1. Molecular Structures of the Dyes DT-1 and DT-2

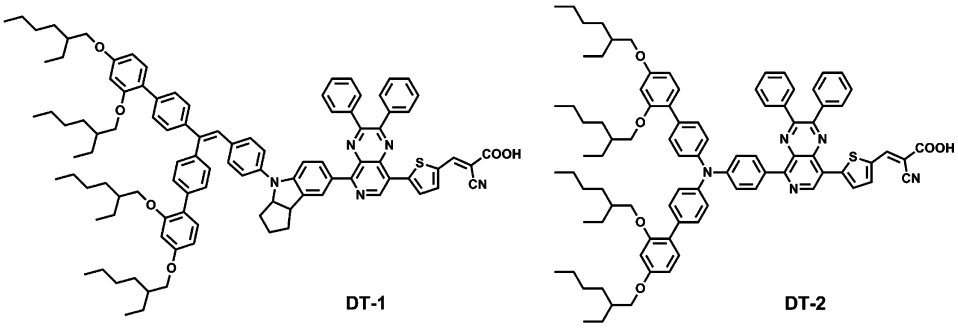

mass transport problems and charge recombination.[31,32] Modifications on the ligands of cobalt complexes and passivation treatments on mesoporous semiconductor layers were carried out in order to reduce the interfacial charge recombination.[33,34] Substantial progress was not made, however, until Hagfeldt et al. published their inspiring work on a new triphenylamine-based organic sensitizer **D35** with *o*,*p*-dibutoxyphenyl as the electron-donating substituent.[35] For the sake of convenience, we here call those bulky donors with the electron-donating *o*,*p*-dialkoxyphenyl substituent as the "Hagfeldt"-type donors. Their work showed a novel and effective approach toward higher photoelectric conversion efficiency with much less charge recombination of electrons in the TiO_2 films and cobalt redox species. Since then, many organic sensitizers with bulky donors have been designed, synthesized and applied to DSSCs with cobalt electrolytes and new record efficiencies keep being refreshed.[36−42] The η of DSSCs based on single organic sensitizer is 10.65%, achieved by employing dye **YA422** with cobalt (II/III) tris-bipyridyl redox electrolyte.[43] **YA422** is a typical organic sensitizer with indoline-based Hagfeldt-type donor. As a matter of fact, "Hagfeldt"-type donors based on indoline and triphenylamine are widely employed to construct D-π-A organic sensitizers for DSSCs with cobalt redox electrolytes.[44−47] However, little research has been conduct to figure out the differences between the two types of bulky donors and their performance in DSSC devices.

Therefore, we constructed two sensitizers with the only difference being in the core of the Hagfeldt-type donor: indoline (**DT-1**) and triphenylamine (**DT-2**). Noticing the absorption onset of **YA422** was only around 670 nm, which posed a limitation to the short-circuit current density (J_{sc} = 15.26 mA cm^{-2} with cobalt electrolyte and J_{sc} = 14.40 mA cm^{-2} with iodide electrolyte),[43] we employed a stronger electron-withdrawing pyrido[3,4-*b*]pyrazine (PP)-based auxiliary acceptor to replace its quinoxaline-based analogue in **YA422** with the aim of further broadening the absorption range and enhancing the J_{sc}.[48] Herein, we report two new D-A-π-A organic sensitizers (**DT-1** and **DT-2**, see Scheme 1) for DSSCs with cobalt electrolytes, consisting of bulky indoline-based or triphenamine-based Hagfeldt-type donors, PP unit as auxiliary acceptor, thiophene as π-bridge and 2-cyanoacetic acid as acceptor and anchoring group. The structure−property relationship of the two dyes was investigated in the DSSC devices with $Co[(bpy)_3]^{3+/2+}$ electrolytes. As a result, DSSCs based on **DT-1** achieved higher photoelectric conversion efficiency of 8.57% under standard AM 1.5 G simulated sunlight (J_{sc} = 16.08 mA cm^{-2}, V_{oc} = 802 mV, and *FF* = 0.66). Electrochemical impedance spectroscopy (EIS) and intensity-modulated photovoltage spectroscopy (IMVS) were employed to investigate the interfacial processes and recombination dynamics in the devices, indicating that **DT-1** with bulky indoline-based Hagfeldt-type donor can retard the charge recombination more effectively, which might be owing to the bigger donor size and the insulating blocking branch in the donor of **DT-1**, as shown by density function theory (DFT) calculations.

EXPERIMENTAL SECTION

Materials and Reagents. Fluorine-doped SnO_2 conducting glass (FTO glass, transparency >90%, sheet resistance 15 Ω/square was obtained from the Geao Science and Educational Co. Ltd. of China. Acetonitrile, tetra-*n*-butyl ammonium hexafluorophosphate ($TBAPF_6$), 4-*tert*-butylpyridine, and lithium iodide were bought from Fluka and iodine (99.999%) was purchased from Alfa Aesar. 5, 8-dibromo-2,3-diphenyl-pyrido[3,4-*b*]pyrazine, compound **1** was synthesized according to the reference.[48] All chemicals and reagents were purchased from suppliers and used without further purification. Tetrahydrofuran (THF) was dried with sodium under argon before use.

Instruments and Characterization. A Brücker AM 400 spectrometer was employed to obtain ^{1}H NMR and ^{13}C NMR spectra with TMS as the internal standard. High resolution mass spectra were obtained via HITACHI-80 mass spectrometer. The UV−vis spectra were measured using a Shimdtzu UV-260 UV−vis spectrometer. A Versastat II electrochemical workstation (Princeton applied research) was utilized to perform cyclic voltammetry measurement on dyes with a three-electrode system, in which glassy carbon electrode as the working electrode, platinum wire as the counter electrode, and a saturated calomel electrode as the reference electrode with ferrocene as the external standard and 0.1 M tetra-*n*-butyl ammonium hexafluorophosphate in dichloromethane as the supporting electrolyte. The scan rate was 50 mV/s.

Synthesis of Sensitizers. *2,5-Dibromopyridine-3,4-diamine (**1**).* Pyridine-3,4-diamine (5.45 g, 50.0 mmol) and 48% HBr (40 mL) was added into a 50 mL flask, followed by slowly adding Br_2 (8 mL) dropwise. Then the mixture was heated at 80 °C for 24h. After cooling, the raw product was collected by filtration and washed using saturated $Na_2S_2O_3$ aqueous solution, saturated $NaHCO_3$ aqueous solution and deionized water successively. In the end, the compound **1** was obtained by recrystallization in ethanol as ochre solid (7.34 g, 55% yield). ^{1}H NMR (400 MHz, $CDCl_3$) δ, ppm: 7.53 (s, 1H), 5.99 (s, 2H), 5.05 (s, 2H).

*5,8-Dibromo-2,3-diphenylpyrido[3,4-b]pyrazine (**2**).* The mixture of compound **1** (2.76 g, 10 mmol), benzil (2.1 g, 10 mmol), and glacial acetic acid (20 mL) was heated at 60 °C for 10h. After it was cooled, the mixture was poured into 500 mL water. The raw product was collected by filtration and purified by chromatography on a silica gel column with CH_2Cl_2/PE (1:1 by volume) to give **2** as yellow solid (2.18 g, 49% yield). ^{1}H NMR (400 MHz, $CDCl_3$) δ, ppm: 8.97 (s, 1H), 7.65 (s, 4H), 7.45 (m, 2H), 7.38 (m, 4H).

*4-(4-(2,2-Bis(2′,4′-bis(octyloxy)-[1,1′-biphenyl]-4-yl)vinyl)phenyl)-7-(8-bromo-2,3-diphenylpyrido[3,4-b]pyrazin-5-yl)-1,2,3,3a,4,8b-hexahydrocyclopenta[b]indole (**3**).* Under an argon atmosphere, a mixture of compound **2** (300 mg, 0.68 mmol) and $Pd(PPh_3)_4$ (24 mg)

DOI: 10.1021/am507824h
ACS Appl. Mater. Interfaces 2015, 7, 2760−2771

in THF (13 mL) was heated to 50 °C. Then 5 mL 2 M K_2CO_3 aqueous solution was added, followed by injecting a solution of (4-(4-(2,2-bis(2′,4′-bis((2-ethylhexyl)-oxy)-[1,1′-biphenyl]-4-yl)vinyl)-phenyl)-1,2,3,3*a*,4,8*b*-hexa-hydrocyclopenta[b]-indol-7-yl)boronic acid (1 mL, 0.5 mmol) in THF slowly. The mixture was heated to 80 °C and refluxed for 8 h. After cooling, the raw product was extracted using CH_2Cl_2 and water. The organic layers were combined and dried by anhydrous Na_2SO_4. After filtration, the solvent was removed under reduced pressure and the residue was purified by chromatography on a silica gel column with CH_2Cl_2/PE (1:1 by volume) to give **3** as red solid (165 mg, 23% yield). ^{1}H NMR (400 MHz, $CDCl_3$) δ, ppm: 8.97 (s, 1H), 8.15 (s, 1H), 8.11 (d, J = 8.8 Hz, 1H), 7.73 (d, J = 7.6 Hz, 2H), 7.62 (d, J = 7.6 Hz, 2H), 7.56 (d, J = 8.0 Hz, 2H), 7.48 (d, J = 8.4 Hz, 2H), 7.40−7.31 (m, 12H), 7.13 (m, 5H), 7,01 (s, 1H), 6.57 (m, 4H), 3.88−3.84 (m, 10H), 2.06−1.90 (m, 4H), 1.76−1.67 (m, 6H), 1.58−1.46 (m, 8H), 1.34−1.26 (m, 24H), 0.97−0.84 (m, 24H).

*5-(5-(4-(4-(2,2-Bis(2′,4′-bis(octyloxy)-[1,1′-biphenyl]-4-yl)vinyl)-phenyl)-1,2,3,3a,4,8b-hexahydrocyclopenta[b]indol-7-yl)-2,3-diphenylpyrido[3,4-b]pyrazin-8-yl)thiophene-2-carbaldehyde (**4**).* Under an argon atmosphere, a mixture of **3** (150 mg, 0.1 mmol) and $Pd(PPh_3)_4$ (18 mg) in THF (12 mL) was heated to 50 °C; then 5 mL of 2 M K_2CO_3 aqueous solution was added, followed by injection of a solution of 5-formyl-2-thiopheneboronic acid (47 mg, 0.3 mmol) in THF (10 mL). Then the mixture was heated to 80 °C and refluxed for 18 h. After it was cooled, the raw product was extracted using CH_2Cl_2 and water. The organic layers were combined and dried by anhydrous Na_2SO_4. After filtration, the solvent was removed under reduced pressure and the residue was purified by chromatography on a silica gel column with CH_2Cl_2/PE (4:1 by volume) to give **4** as red solid (112 mg, 73% yield). ^{1}H NMR (400 MHz, $CDCl_3$) δ, ppm: 10.00 (s, 1H), 9.25 (s, 1H), 8.27 (s, 1H), 8.24 (d, J = 8.8 Hz, 1H), 7.97 (d, J = 4.0 Hz, 1H), 7.86 (d, J = 4.0 Hz, 1H), 7.78 (d, J = 6.4 Hz, 2H), 7.66 (d, J = 6.8 Hz, 2H), 7.56 (d, J = 8.0 Hz, 2H), 7.46 (dd, J = 8.4 Hz, J = 16.4 Hz, 6H), 7.39−7.36 (m, 4H), 7.34−7.31 (m, 4H), 7.14 (m, 5H), 7.02 (s, 1H), 6.57 (m, 4H), 3.88 (m, 10H), 2.03−1.97 (m, 4H), 1.75−1.68 (m, 6H), 1.43−1.42 (m, 8H), 1.33 (m, 24H), 0.93−0.86 (m, 24H).

*(E)-3-(5-(5-(4-(4-(2,2-Bis(2′,4′-bis(octyloxy)-[1,1′-biphenyl]-4-yl)-vinyl)phenyl)-1,2,3,3a,4,8b-hexa-hydrocyclopenta[b]indol-7-yl)-2,3-diphenylpyrido-[3,4-b]pyrazin-8-yl)thiophen-2-yl)-2-cyanoacrylic acid (**DT-1**).* Under an argon atmosphere, a mixture of **4** (111 mg, 0.075 mmol), 2-cyanoacetic acid (85 mg, 1 mmol), and ammonium acetate (115 mg, 1.5 mmol) in acetic acid (13 mL) was refluxed at 120 °C for 12 h. After it was cooled, the mixture was poured into 300 mL saturated NaCl aqueous solution and stirred. The precipitate was collected by filtration and purified by chromatography on a silica gel column with CH_2Cl_2/methanol (20:1 by volume) to give **DT-1** as black solid (89 mg, 77% yield). ^{1}H NMR (400 MHz, $CDCl_3$) δ, ppm: 10.77 (s, 1H), 8.30 (m, 2H), 7.93 (m, 4H), 7.47−7.45 (m, 4H), 7.36−7.34 (m, 3H), 7.27−7.25 (m, 3H), 7.19−7.18 (m, 5H), 7.11−7.07 (m, 8H), 6.95 (s, 2H), 6.50 (m, 2H), 6.44 (m, 3H), 3.78 (m, 10H), 2.00−1.73 (m, 6H), 1.28−1.18 (m, 36H), 0.85−0.76 (m, 24H). ^{13}C NMR (100 MHz, $CDCl_3$) δ, ppm: 160.62, 157.66, 131.28, 130.29, 129.58, 127.18, 123.30, 105.71, 100.47, 71.70, 70.89, 70.73, 39.88, 39.81, 39.74, 31.53, 30.93, 30.34, 30.09, 29.52, 29.45, 29.36, 24.45, 24.27, 23.50, 23.43, 14.29, 11.32, 11.22. HRMS (ESI) m/z: $[M + H]^+$ calcd for $C_{102}H_{114}N_5O_6S$, 1536.8490; found, 1536.8488.

*4-(8-Bromo-2,3-diphenylpyrido[3,4-b]pyrazin-5-yl)-N,N-diphenyl-aniline (**5**).* Under an argon atmosphere, a mixture of **2** (882 mg, 2 mmol) and $Pd(PPh_3)_4$ (22 mg) in THF (15 mL) was heated to 50 °C, then 5 mL of 2 M K_2CO_3 aqueous solution was added, followed by injecting a solution of 4-(diphenylamino)phenylboronic acid (289 mg, 1 mmol) in THF slowly. Then the mixture was heated to 65 °C and refluxed for 8 h. After it was cooled, the raw product was extracted using CH_2Cl_2 and water. The organic layers were combined and dried by anhydrous Na_2SO_4. After filtration, the solvent was removed under reduced pressure, and the residue was purified by chromatography on a silica gel column with CH_2Cl_2/PE (1:1 by volume) to give **5** as orange red solid (478 mg, 79% yield). ^{1}H NMR (400 MHz, $CDCl_3$) δ, ppm: 9.03 (s, 1H), 8.24−8.22 (m, 2H), 7.72 (m, 2H), 7.59 (m, 2H), 7.39−7.26 (m, 14H), 7.20 (m, 2H), 7.11−7.09 (m, 2H).

*5-(5-(4-(Diphenylamino)phenyl)-2,3-diphenyl-pyrido[3,4-b]-pyrazin-8-yl)thiophene-2-carbaldehyde (**6**).* Under an argon atmosphere, a mixture of **5** (200 mg, 0.33 mmol) and $Pd(PPh_3)_4$ (16 mg) in THF (12 mL) was heated to 50 °C, then 5 mL of 2 M K_2CO_3 aqueous solution was added, followed by injecting a solution of 5-formyl-2-thiopheneboronic acid (156 mg, 1 mmol) in THF (10 mL) was added. Then the mixture was heated to 80 °C and refluxed for 16 h. After cooling, the raw product was extracted using CH_2Cl_2 and water. The organic layers were combined and dried by anhydrous Na_2SO_4. After filtration, the solvent was removed under reduced pressure and the residue was purified by chromatography on a silica gel column with CH_2Cl_2/PE (2:1 by volume) to give **6** as red solid (153 mg, 73% yield). ^{1}H NMR (400 MHz, $CDCl_3$) δ, ppm: 10.00 (s, 1H), 9.28 (s, 1H), 8.36 (s, 1H), 8.34 (s, 1H), 7.98 (d, J = 4.4 Hz, 1H), 7.86 (d, J = 4.0 Hz, 1H), 7.75 (d, J = 6.4 Hz, 2H), 7.62 (d, J = 6.8 Hz, 2H), 7.44−7.42 (m, 2H), 7.37−7.30 (m, 7H), 7.23−7.22 (m, 3H), 7.21−7.20 (m, 3H), 7.12−7.09 (m, 3H).

*5-(5-(4-(Bis(4-iodophenyl)amino)phenyl)-2,3-diphenylpyrido[3,4-b]pyrazin-8-yl)thiophene-2-carbaldehyde (**7**).* Under an argon atmosphere, a mixture of **6** (388 mg, 0.61 mmol), KI (607 mg, 3.66 mmol), acetic acid (30 mL), and H_2O (3 mL) was heated to 80 °C. Then KIO_3 (522 mg, 2.44 mmol) was added, and the mixture was stirred for 8 h. After it was cooled, the mixture was poured into 500 mL saturated NaCl aqueous solution and stirred, followed by extraction with CH_2Cl_2 and water. After removal of the solvent under reduced pressure, the residue was purified by chromatography on a silica gel column with CH_2Cl_2/PE (3:1 by volume) to give **7** as dark red solid (236 mg, 44% yield). ^{1}H NMR (400 MHz, $CDCl_3$) δ, ppm: 10.01 (s, 1H), 9.30 (s, 1H), 8.36 (d, J = 8.8 Hz, 2H), 7.99 (d, J = 4.0 Hz, 1H), 7.87 (d, J = 4.0 Hz, 1H), 7.76−7.74 (m, 2H), 7.62−7.58 (m, 6H), 7.44−7.42 (m, 4H), 7.38−7.36 (m, 2H), 7.22−7.20 (m, 2H), 6.96−6.94 (m, 4H).

*5-(5-(4-(Bis(2′,4′-bis(octyloxy)-[1,1′-biphenyl]-4-yl)amino)-phenyl)-2,3-diphenylpyrido[3,4-b]pyrazin-8-yl)thiophene-2-carbaldehyde (**8**).* Under an argon atmosphere, a mixture of **7** (311 mg, 0.35 mmol) and $Pd(PPh_3)_4$ (25 mg) in THF (14 mL) was heated to 50 °C, then 5 mL 2 M K_2CO_3 aqueous solution was added, followed by injecting a solution of (2,4-bis(octyloxy)phenyl)-boronic acid (3 mL, 1.5 mmol) in THF was added. Then the mixture was heated to 80 °C and refluxed for 18 h. After it was cooled, the raw product was extracted using CH_2Cl_2 and water. The organic layers were combined and dried by anhydrous Na_2SO_4. After filtration, the solvent was removed under reduced pressure, and the residue was purified by chromatography on a silica gel column with CH_2Cl_2/PE (3:1 by volume) to give **8** as purplish red solid (325 mg, 71% yield). ^{1}H NMR (400 MHz, $CDCl_3$) δ, ppm: 10.03 (s, 1H), 9.32 (s, 1H), 8.41 (d, J = 8.8 Hz, 2H), 8.01 (d, J = 4.0 Hz, 1H), 7.88 (d, J = 4.0 Hz, 1H), 7.79 (d, J = 6.4 Hz, 2H), 7.67 (d, J = 6.8 Hz, 2H), 7.52−7.42 (m, 8H), 7.41−7.36 (m, 4H), 7.34−7.31 (m, 3H), 7.28 (m, 3H), 6.61−6.59 (m, 4H), 3.93−3.90 (m, 8H), 1.80−1.73 (m, 4H), 1.45−1.30 (m, 32H), 0.99−0.89 (m, 24H).

*(E)-3-(5-(5-(4-(Bis(2′,4′-bis(octyloxy)-[1,1′-biphenyl]-4-yl)amino)-phenyl)-2,3-diphenylpyrido[3,4-b]pyrazin-8-yl)thiophen-2-yl)-2-cyanoacrylic acid (**DT-2**).* **DT-2** was synthesized in a similar way to **DT-1** by compound **4** with compound **8**. The residue was purified by chromatography on a silica gel column with CH_2Cl_2/methanol (20:1 by volume) to give **DT-2** as black solid (130 mg, 77% yield). ^{1}H NMR (400 MHz, $CDCl_3$) δ, ppm: 10.77 (s, 1H), 8.28 (m, 3H), 7.92 (m, 2H), 7.48 (m, 2H), 7.36−7.33 (m, 6H), 7.18−7.13 (m, 4H), 7.09−7.05 (m, 10H), 6.48 (m, 2H), 6.37−6.36 (m, 2H), 3.75 (m, 8H), 1.59−1.52 (m, 4H), 1.29−1.18 (m, 32H), 0.86−0.74 (m, 24H). ^{13}C NMR (100 MHz, $CDCl_3$) δ, ppm: 159.91, 157.19, 145.38, 130.59, 130.34, 124.13, 122.98, 105.09, 100.10, 70.38, 69.84, 53.93, 39.66, 39.49, 29.68, 28.94, 23.80, 22.97, 13.55, 13.53, 10.58. HRMS (ESI) m/z: $[M + H]^+$ calcd for $C_{89}H_{102}N_5O_6S$, 1368.7551; found, 1368.7544

Fabrication of DSSCs. A compact TiO_2 layer was first deposited on the FTO glass by immersing into 40 mM $TiCl_4$ aqueous solution at 70 °C for 30 min three times and sintered at 450 °C for 30 min. Then

DOI: 10.1021/am507824h
ACS Appl. Mater. Interfaces 2015, 7, 2760−2771

Scheme 2. Synthetic routes of Dyes DT-1 and DT-2[a]

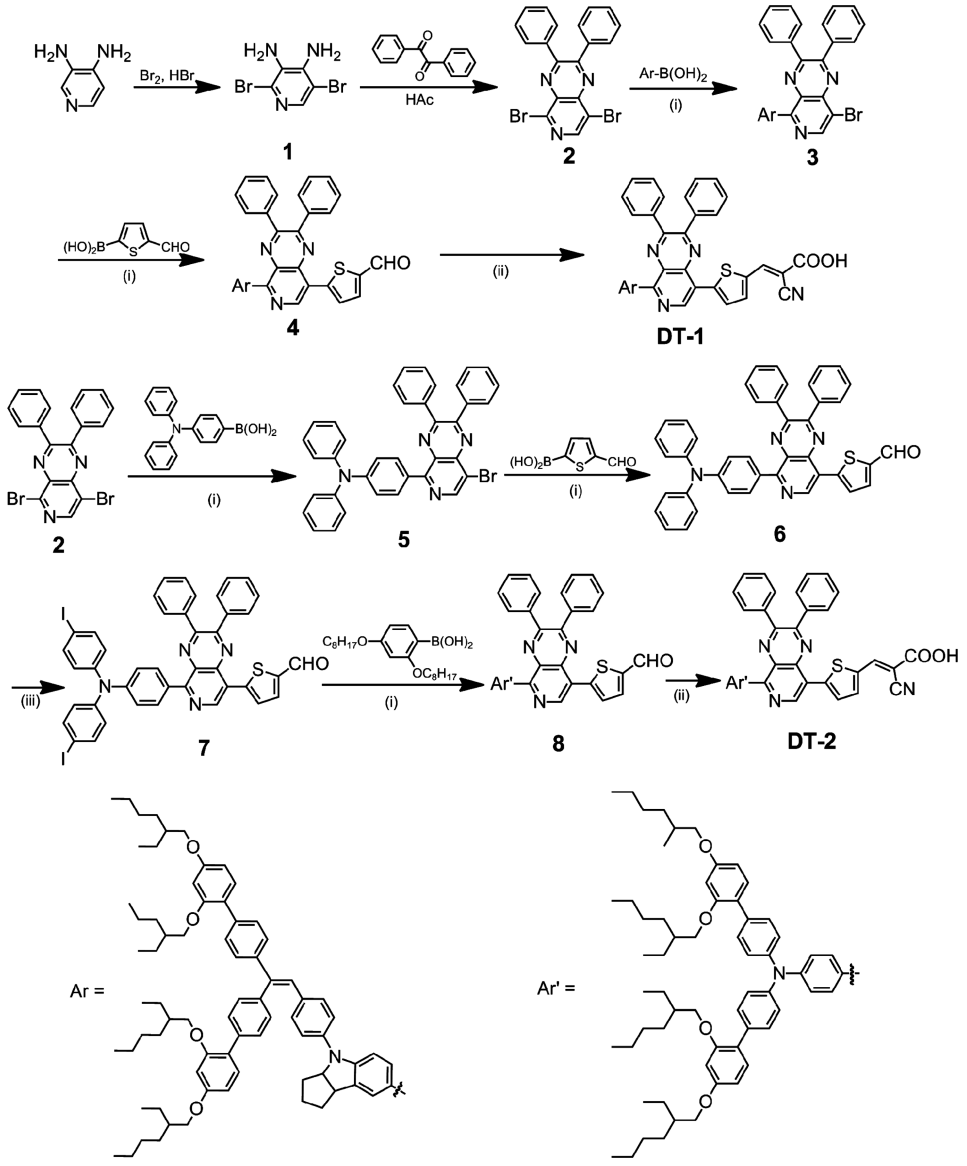

[a](i) $Pd(PPh_3)_4$, K_2CO_3, THF/H_2O. (ii) Cyanoacetic acid, NH_4OAc, AcOH. (iii) KI, KIO_3, AcOH, H_2O.

one layer of Dyesol 90-T TiO_2 paste and a scattering layer were screen-printed onto and sintered gradually up to 500 °C and kept at this temperature before cooling. The photoanodes were immersed into 40 mM $TiCl_4$ aqueous solution at 70 °C for 30 min and sintered at 450 °C for 30 min again. Then the photoanodes were placed into 3×10^{-4} M dye bath in $CH_3CH_2OH/CHCl_3$ = 1:1(v/v) solution for 6 h. The dye-sensitized photoanodes were sealed with platinized counter electrodes by a hot-melt film (25-μm-thick Surlyn, Dupont). The electrolytes were introduced to the cells via two predrilled holes in the counter electrodes. The cobalt electrolyte consists of 0.22 M $[Co(II)(bpy)_3]TFSI_2$, 0.06 M $[Co(III)(bpy)_3]TFSI_3$, 0.1 M LiTFSI, and 0.5 M *tert*-butylpyridine in acetonitrile. The active area of all DSSCs is 0.25 cm^2.

Photovoltaic Property Measurements. The current−voltage photovoltaic characterization was performed using the setup consisting of a 450 W xenon lamp (Oriel), a Schott K113 Tempax sunlight filter (PräzisionsGlas & Optik GmbH), and a Keithley 2400 source meter which applies potential bias and measures the photogenerated current. A set of circular variable neutral density filters used to adjust the light intensity was brought from Unice E-O Services Inc. in Taiwan. Monochromatic incident photon-to-current conversion efficiency (IPCE) was obtained via the setup using a SR830 lock-in amplifier, a 300 W xenon lamp (ILC Technology) and a Gemini-180 double monochromator (Jobin-Yvon Ltd.). A Zahner IM6e Impedance Analyzer (ZAHNER-Elektrik GmbH & CoKG, Kronach, Germany) was employed to carry out the electrochemical impedance spectroscopy. The frequency range was 0.1 Hz−100 kHz and the applied bias was from −0.05 to −0.95 V. The magnitude of the alternating signal was 5 mV. Intensity-modulated photovoltage spectroscopy was performed on the Zahner IM6e Impedance Analyzer (ZAHNER-Elektrik GmbH & CoKG, Kronach, Germany) with a light-emitting display array (λ = 457 nm, blue light). The frequency range was also 0.1 Hz−100 kHz.

RESULTS AND DISCUSSION

Synthesis. The synthetic routes of **DT-1** and **DT-2** are depicted in Scheme 2. We can see that the synthesis of **DT-1** and **DT-2** started from two Suzuki coupling reactions with 5, 8-dibromo-2,3-diphenylpyrido[3,4-*b*]pyrazine (**2**) and resulted in the corresponding aldehyde precursors (**4** and **6**). The indoline-based bulky donor part was synthesized according to

DOI: 10.1021/am507824h
ACS Appl. Mater. Interfaces 2015, 7, 2760−2771

other literatures.[43] The triphenylamine-based bulky donor unit was synthesized in two steps. It started from the aldehyde precursor **7**, as shown in Scheme 2, followed with the Suzuki reaction to couple with the 2,4-bis((2-ethylhexyl)oxy)benzene group and resulted in the aldehyde **8**. The final reaction was condensation of the aldehyde (**4** or **8**) with cyanoacetic acid by the Knoevenagel reaction to produce **DT-1** and **DT-2**. All key intermediates were characterized with ^{1}H NMR and organic pyrido[3,4-*b*]pyrazine-based sensitizers were fully characterized with ^{1}H NMR, ^{13}C NMR, and HRMS in the Experimental Section.

Photophysical Properties. The absorption spectra of **DT-1** and **DT-2** in CH_2Cl_2 solution and on TiO_2 films are shown in Figure 1 and the related data can be found in Table 1.

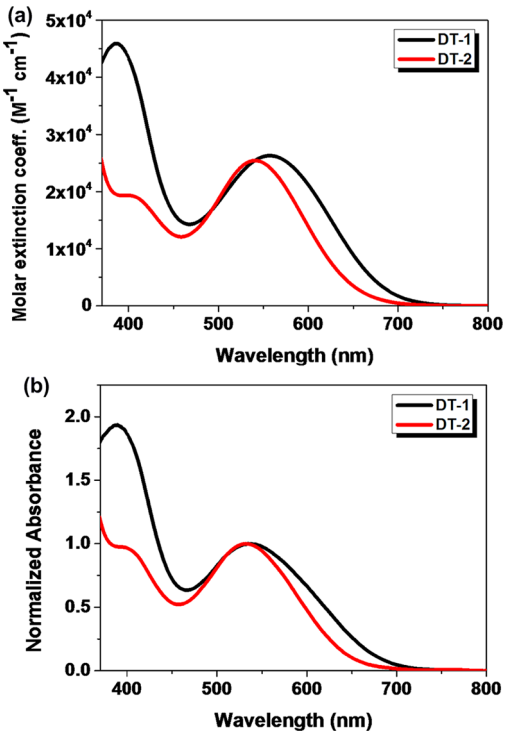

Figure 1. Absorption spectra of **DT-1** and **DT-2** in CH_2Cl_2 solution (a) and adsorbed on TiO_2 transparent films (b).

Table 1. Optical and Electrochemical Properties of the Dyes DT-1 and DT-2

dye	λ_{max}[a] (nm) ($\varepsilon \times 10^4$ M^{-1} cm^{-1})	λ_{max}[b] (nm)	HOMO[c] (V vs NHE)	E_{0-0}[d] (eV)	LUMO[e] (V vs NHE)
DT-1	557 (2.63)	540	0.90	1.84	−0.94
DT-2	541 (2.55)	532	0.92	1.89	−0.97

[a]Absorption maximum in CH_2Cl_2 solution (1.5×10^{-5} M). [b]Absorption maximum on 4 μm TiO_2 transparent films. [c]HOMOs were measured in CH_2Cl_2 with 0.1 M tetra-*n*-butylammonium hexafluorophosphate ($TBAPF_6$) as electrolyte (working electrode, Pt; reference electrode:, SCE; counter electrode, Pt wire; calibrated with ferrocene/ferrocenium (Fc/Fc^+) as an external reference (0.69 V vs NHE).). [d]E_{0-0} was estimated from the absorption thresholds from UV−vis absorption spectra of the dyes. [e]LUMO was estimated by subtracting E_{0-0} from E_{HOMO}.

According to Figure 1a, both **DT-1** and **DT-2** in CH_2Cl_2 exhibit two major absorption bands, appearing at 370−470 and 470−700 nm. Compared to the absorption onset of **YA422** (~630 nm),[43] the absorption onsets of **DT-1** and **DT-2** red-shifted significantly to ~700 nm, which indicates that the auxiliary acceptor with strong electron-withdrawing capability can effectively broaden the spectral response range. The absorption band at shorter wavelength can be ascribed to the localized aromatic $\pi-\pi^*$ transition from the donor group to the PP moiety. Meanwhile, the absorption band at longer wavelength can be attributed to the intramolecular charge transfer (ICT) transition from the donor group to the cyanoacetic acceptor unit. The absorption spectra of the two dyes exhibit absorption maxima at 557 (**DT-1**) (ε = 2.63 × 10^4 M^{-1} cm^{-1}) and 541 nm (**DT-2**) ($\varepsilon = 2.55 \times 10^4$ M^{-1} cm^{-1}), respectively. Apparently, the observed bathochromic shift of 16 nm by **DT-1** can be attributed to the stronger electron-donating capability of the indoline unit than that of triphenylamine, which is consistent with our previous work.[49] Simultaneously, the absorption range is also extended a bit by the indoline donor, suggesting that the indoline unit can narrow the bandgap and optimize the energy levels more efficiently than the triphenylamine unit, which is beneficial to light-harvesting and the whole photoelectric conversion efficiency. Compared to the absorption spectra in the solution, the maximum absorption peaks for **DT-1** and **DT-2** on 4 μm TiO_2 transparent films (see Figure 1b) are slightly blue-shifted to 540 and 532 nm, respectively, which may be ascribed to the deprotonation of the carboxylic acid.[50]

Electrochemical Properties. To investigate the feasibility of electron injection from excited dyes into the conduction band of TiO_2 and dye regeneration by redox electrolyte of **DT-1** and **DT-2,** cyclic voltammetry (CV) was carried out with a three-electrode system in which a glassy carbon electrode was used as working electrode, platinum wire as counter electrode and saturated calomel electrode (SCE) as reference electrode. Ferrocene/ferrocenium (Fc/Fc^+) was employed as an external reference and tetra-*n*-butylammonium hexafluorophosphate in CH_2Cl_2 (0.1 M) as supporting electrolyte. The CV plots of **DT-1** and **DT-2** are given in Supporting Information Figure S1. All the parameters of electrochemical properties are collected in Table 1. The redox potentials in the CV plots correspond to the highest occupied molecular orbital (HOMO) energy levels of **DT-1** and **DT-2**, presenting as 0.90 and 0.92 V vs NHE, respectively, which are more positive than the redox potentials of I^-/I_3^- (~0.4 V vs NHE) and $[Co(bpy)^3]^{2+}/[Co(bpy)^3]^{3+}$ (0.56 V vs NHE), suggesting sufficient driving forces for dye regeneration. Furthermore, the small upward shift of HOMO level of **DT-2** indicates that the indoline-based unit has stronger electron-donating capability than that of the triphenylamine-based analogue. Estimated from the absorption thresholds of the dyes, the band gap energies (E_{0-0}) of **DT-1** and **DT-2** are 1.84 and 1.89 eV, respectively. Calculated by subtracting E_{0-0} from E_{HOMO}, the lowest unoccupied molecular orbital (LUMO) energy levels **DT-1** and **DT-2** are −0.94 and −0.97 V, respectively. The LUMO levels of these dyes are considerably more negative than the conduction band edge energy level (E_{CB}) of the TiO_2 semiconductor (−0.5 V vs. NHE), indicating sufficient driving forces for electron injection from the excited dye molecules to the TiO_2 conduction band. Therefore, these two sensitizers are qualified to be used in DSSCs in theory.

DFT Calculations. To gain insight into the molecular structure and electron distribution of the sensitizer dyes, **DT-1** and **DT-2**, the ground state geometries were optimized by density functional theory (DFT) calculations employing the hybrid B3LYP functional and the 6-31G(d) basis set.[51−53]

DOI: 10.1021/am507824h
ACS Appl. Mater. Interfaces 2015, 7, 2760−2771

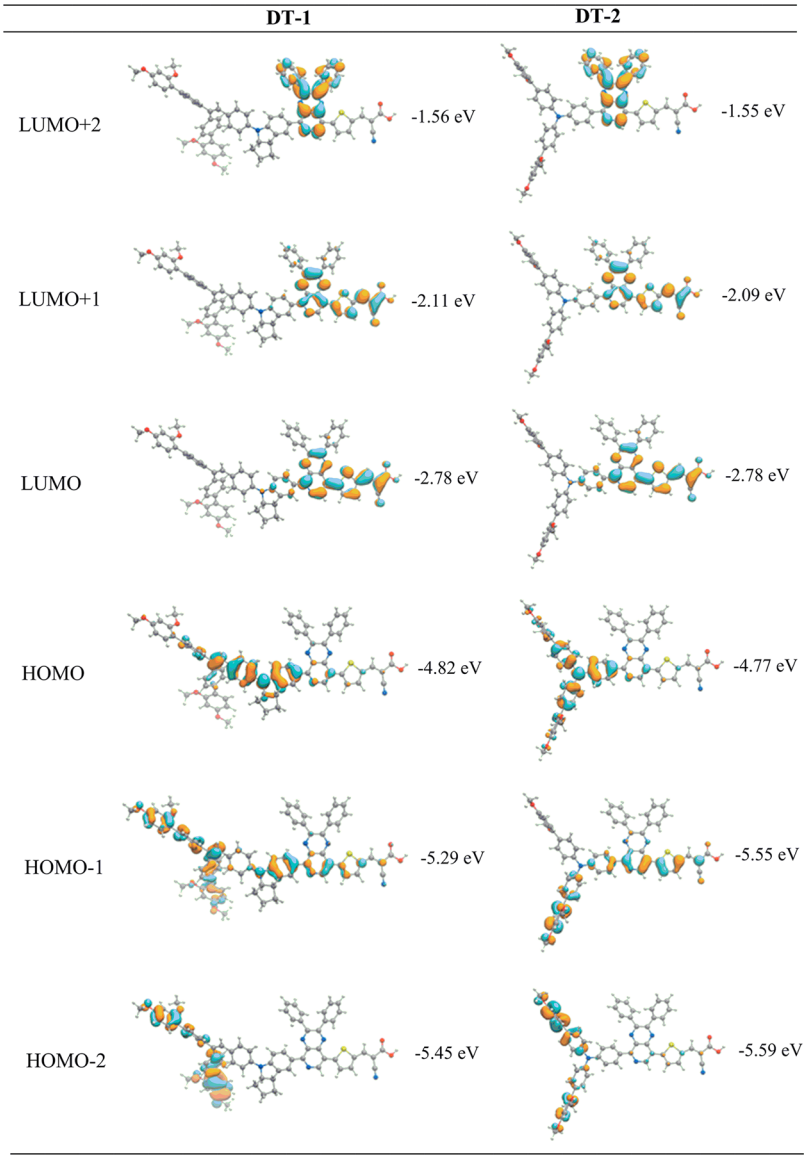

Figure 2. Computed energy levels and the spatial distribution of the frontier molecular orbitals of **DT-1** and **DT-2**.

In the calculations, the long alkoxyl chains were replaced by methoxyl groups to reduce computational costs without affecting the nature of frontier molecular orbitals. At the optimized geometries, time-dependent (TD) DFT calculations were carried out to shed light on the low-lying excited states of the sensitizer dyes, using the range-separated CAM-B3LYP functional and the triple-ζ TZVP basis set.[54,55] All theoretical calculations were carried out using the Gaussian 09 program package.[56]

The computed energy levels and the spatial distribution of the frontier molecular orbitals of **DT-1** and **DT-2** are shown in Figure 2. We can see that the virtual orbitals (LUMO, LUMO + 1, and LUMO + 2) in these two sensitizer dyes are on almost identical energy levels, since they possess the same acceptor moieties. Differences arise in the occupied orbitals, where the HOMO − 1 and HOMO − 2 of **DT-1** reside on closer energy levels to the HOMO, compared to **DT-2**. As for their spatial distribution, the LUMO and LUMO + 1 are both located on the acceptor groups, while the LUMO + 2 resides on the central electron-deficient unit. The HOMO and HOMO − 2 are located on different parts of the donor moieties, while the HOMO − 1 is delocalized over the whole molecule. In addition, it was found that the HOMO and HOMO − 1 of **DT-1** receive more contributions from one biphenyl branch of large indoline-based donor moiety than the other, which is in the *trans*-position of the *N*-phenylindoline unit. The biphenyl branch in the *cis*-position contributes less to the HOMO and HOMO−1 of **DT-1**, which are important orbitals that participate in the absorption of visible light. This can be ascribed to the fact that the *cis*-position is adverse to electron transfer from the biphenyl branch to *N*-phenylindoline. We would also like to emphasis that the HOMO of **DT-1** is rather localized on the indoline core and the adjacent ethylene moiety with less contribution from the alkoxyphenyl branches, in contrast to that of **DT-2**. Similar bad electronic communication between branches and the core of donor moiety was found by Gabriela Marzari et al. when they attached perfluoroalkoxy groups on the donor part of fluorene-bridged sensitizers.[57] They suggested that perfluoroalkoxy groups mainly exhibit the antiaggregation properties, and possibly shield TiO_2 surface to reduce the back electron transfer to the electrolyte, which was evidenced by the corresponding photovoltaic performance of

DOI: 10.1021/am507824h
ACS Appl. Mater. Interfaces 2015, 7, 2760−2771

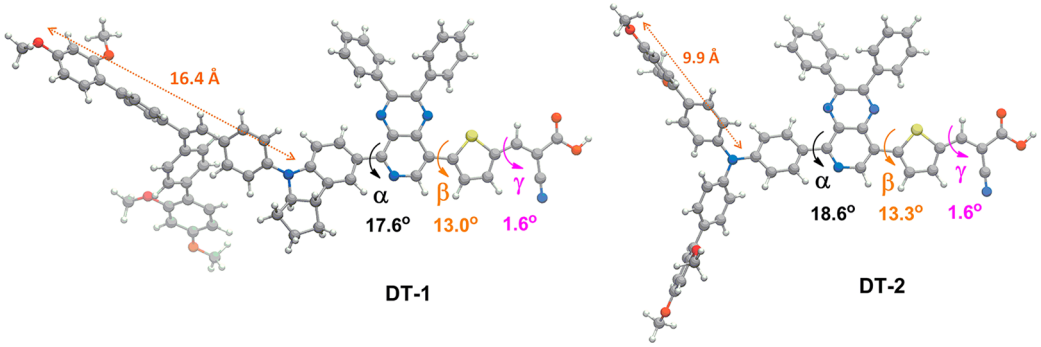

Figure 3. Dihedral angles and the donor sizes of **DT-1** and **DT-2**.

sensitizers.[57] In our case, the biphenyl branch at the *cis*-position of **DT-1** could also act like an insulating block unit to inhibit the dye aggregation and charge recombination at the interface of TiO_2/dye/electrolyte. While for **DT-2**, its HOMO resides evenly on the two biphenyl branches of the large triphenylamine-based donor segment and is extended to the peripheral alkoxyphenyl moieties, which is expected to be less effective in suppressing charge recombination.

Supporting Information Figure S3 illustrates the theoretical absorption spectra provided by TD-DFT calculations. The simulated absorption spectra show qualitative agreement with experimental results, albeit the excitation energies are overestimated. The main absorption peaks in the visible region arise from the HOMO → LUMO transition which corresponds to charge transfer from the donor to the acceptor moieties (Supporting Information Table S2). The strong absorption bands at shorter wavelengths arise from electronic transitions from HOMO to higher virtual orbitals, for instance LUMO + 3 for **DT-1** and LUMO + 4 for **DT-2**, which correspond to local excitations of the donor units (see Supporting Information Figure S4).Because of its larger π-conjugation, the local excitation energy of the donor of **DT-1** is lower than that of **DT-2**, in agreement with experimental observation.

The dihedral angles between donor moiety to PP group (α), between PP group and thiophene unit (β) and between thiophene unit and 2-cyanopyridine moiety (γ), as well as the sizes of the donors are illustrated in Figure 3. We can see that **DT-1** and **DT-2** have similar values in the three dihedral angles, owing to their similarities in molecular structures. Therefore, the replacement of indoline-based donor with triphenylamine donor does not evidently influence the planarity of the whole molecule, which proved that the molecular planarity does not contribute to the bathochromic shift of absorption maxima of **DT-1** and **DT-2**. In addition, the small dihedral angles (less than 20°) not only are beneficial for ICT process but also can increase the likelihood of dye aggregation on the TiO_2 films. The sizes of the donors, which were evaluated by the distance between the methoxyl group and the phenyl nitrogen atom, are 16.4 and 9.9 Å in **DT-1** and **DT-2**, respectively, reflecting the larger donor size of dye **DT-1**.

Photovoltaic Performance. The DSSCs performances of all the dyes were tested under AM 1.5G irradiation (1 sun, 100 mW cm^{-2}). Considering that the HOMO levels of **DT-1** and **DT-2** are 0.88 and 0.90 V vs NHE, respectively, $[Co(bpy)_3]^{2+/3+}$ redox electrolyte was employed in DSSCs based on the dye **DT-1** and **DT-2** to reduce the loss in potential. The composition of the cobalt electrolyte used in this study is 0.22 M $[Co(II)(bpy)_3]$-$TFSI_2$, 0.06 M $[Co(III)(bpy)_3]TFSI_3$, 0.1 M LiTFSI, and 0.5 M *tert*-butylpyridine (TBP) in acetonitrile (TFSI = bis-(trifluoromethylsulfonyl)imide). IPCE spectra for DSSCs based on **DT-1** and **DT-2** in cobalt electrolyte are shown in Figure 4. Both dyes exhibit high IPCE values of more than 75%

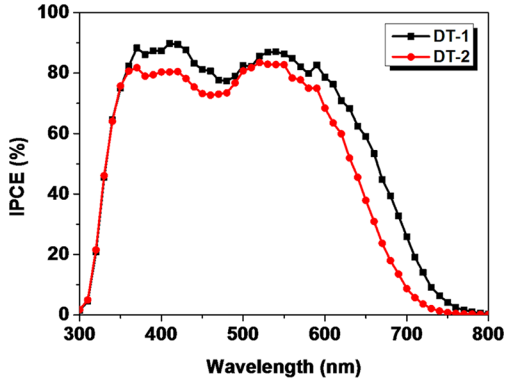

Figure 4. IPCE spectra for DSSCs based on **DT-1** and **DT-2** with cobalt electrolyte.

in the range of 350−600 nm. The broader wavelength range of IPCE and higher IPCE values suggest that **DT-1** should have higher J_{sc} than that of **DT-2**.

The J−V curves of DSSCs based on **DT-1** and **DT-2** with cobalt redox electrolyte under simulated AM 1.5G irradiation are given in Figure 5. We can see that the DSSC sensitized by

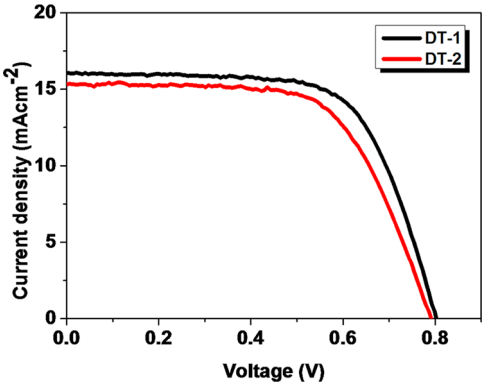

Figure 5. Current−voltage characteristics of DSSCs based on **DT-1** and **DT-2**.

DT-1 clearly outperforms the device based on the **DT-2** mostly because of a higher J_{sc}. All the photoelectric results of J−V measurement of DSSCs based on **DT-1** and **DT-2** with cobalt

DOI: 10.1021/am507824h
ACS Appl. Mater. Interfaces 2015, 7, 2760−2771

Table 2. Photovoltaic Performance of the DT-1 and DT-2-Based DSSCs with Cobalt Redox System at Different Incident Light Intensity[a]

dye	incident light intensity I_0 (mW cm^{-2})	J_{sc} (mA cm^{-2})	V_{oc} (mV)	FF	η (%)
DT-1	100	16.08	802	0.66	8.57
	80	13.02	784	0.66	8.43
	63.1	9.87	774	0.68	8.22
	50	7.27	760	0.68	7.50
	31.6	5.23	748	0.70	8.59
	10	1.48	693	0.71	7.26
DT-2	100	15.35	790	0.64	7.74
	80	11.87	788	0.68	8.04
	63.1	8.74	778	0.71	7.60
	50	6.73	768	0.72	7.40
	31.6	4.54	752	0.73	7.89
	10	1.31	700	0.74	6.79

[a]Electrolyte: 0.22 M [Co(II)(bpy)$_3$]TFSI$_2$, 0.06 M [Co(III)(bpy)$_3$]-TFSI$_3$, 0.1 M LiTFSI, and 0.5 M *tert*-butylpyridine (TBP) in acetonitrile.

redox electrolyte under different incident light intensities are tabulated in Table 2. We further investigate the mass transport of redox species and charge recombination kinetics in DSSCs based on **DT-1** and **DT-2** via the method of EIS and IMVS. The photocurrent density behaviors of DSSCs based on **DT-1** and **DT-2** under different incident light intensities are illustrated in Figure 6. We can see that the J_{sc} values of DSSCs

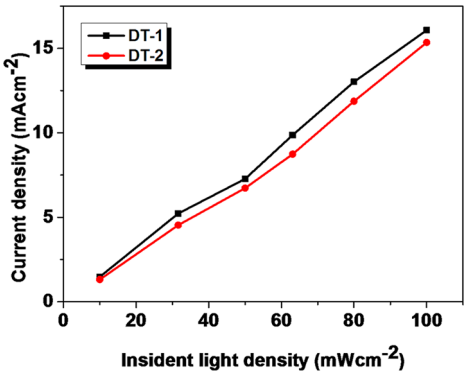

Figure 6. Photocurrent density behaviors of DSSCs based on **DT-1** and **DT-2** under different incident light intensities.

based on **DT-1** and **DT-2** with cobalt redox electrolyte increased linearly with incident light intensities, suggesting that there are little mass transport problems in the DSSCs devices.[25] In the end, we achieved the highest PCE of 8.57% by DSSCs based on **DT-1** at AM 1.5 G simulated sunlight, with J_{sc} = 16.08 mA cm^{-2}, V_{oc} = 802 mV, and FF = 0.66. Furthermore, DSSCs based on **DT-1** and **DT-2** with cobalt redox electrolyte show higher J_{sc}s than that of **YA422** (15.26 mA cm^{-2}, platinized counter electrode),[43] suggesting the benefits of introducing the strongly electron-withdrawing PP unit.

Photovoltaic performance of DSSCs based on **DT-1** and **DT-2** with iodide electrolyte are provided in the Supporting Information for reference (Figure S2 and Table S1). We can see that the V_{oc} values of DSSCs based on **DT-1** and **DT-2** with iodide electrolyte are very low before coadsorbed with CDCA (<650 mV). At the presence of 5 mM CDCA, the V_{oc} values are enhanced by 40−70 mV, and the J_{sc} values are improved, particularly for DSSC based on **DT-2** (from 8.96 to 14.99 mA cm^{-2}), indicating more serious dye aggregation problems for **DT-2** than **DT-1**. The manifestly different influence caused by the coadsorption of CDCA with **DT-2** and **DT-1** on the performance of DSSCs is a strong indication that the bulky indoline-based donor group has greater steric hindrance than the triphenylamine moiety, which can prevent dye aggregation more efficiently. Moreover, the IPCE values of DSSCs based on **DT-1** are higher than that of their counterparts with **DT-2** throughout the whole wavelength range, providing explanation for the higher J_{sc} and PCE. The PCEs of DSSCs based on **DT-1** and **DT-2** with iodide electrolyte are not very high, being lower than their counter parts with cobalt electrolyte.

Electrochemical Impedance Spectroscopy. Electrochemical impedance spectroscopy (EIS) was utilized as a common tool to investigate interfacial charge transfer and recombination processes.[58−60] The dark currents in DSSCs based on **DT-1** and **DT-2** with cobalt electrolyte against the IR drop corrected potential were presented in Figure 7. The EIS

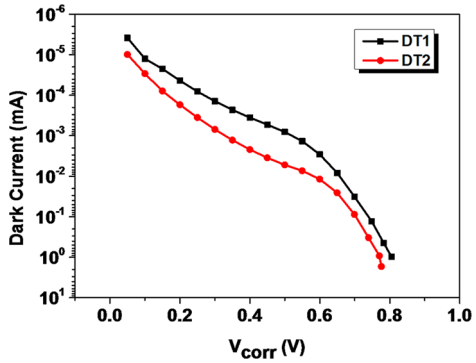

Figure 7. Dark currents of DSSCs based on **DT-1** and **DT-2** with cobalt electrolyte against the IR drop corrected potential.

measurements were performed in the dark and the applied bias voltage was from −0.05 to −0.95 V. Data were fitted using the transmission line model.[61−63] The smaller dark current in DSSC based on **DT-1** indicates less charge recombination between TiO_2 surface and electrolyte and less loss of current in device, which can partly explain the higher J_{sc} and V_{oc} of DSSC based on **DT-1**.

Figure 8 depicts the charge transfer resistance (R_{ct}) and chemical capacitance (C_{chem}) of **DT-1** and **DT-2** based DSSCs as functions of IR drop corrected potential. Inset shows their charge transport resistance (R_{trans}). In the case of DSSCs with cobalt electrolyte, since the mesoporous TiO_2 films are insulating at lower bias voltages, the R_{ct} represents the charge transfer resistance between the FTO substrate and the electrolyte. As the applied bias increases, the mesoporous TiO_2 films become increasingly conductive. Therefore, R_{ct} values at intermediate- and higher- biases represent the charge transfer resistance between the mesoporous TiO_2 films and the electrolyte.[64] In Figure 8, we can see clearly that the R_{ct} values in DSSCs based on **DT-1** are 2−3 times larger than those based on **DT-2**. Such a big difference in the ability of retarding charge recombination arises from the only structural difference in the core of bulky donor between **DT-1** and **DT-2**, demonstrating the great importance of fine molecular design of sensitizers to the device performance of DSSCs. The C_{chem} can describe the exponential trap distribution below the conduction band edge and has a close relationship with the Fermi level. At the potentials near the V_{oc}, the C_{chem} values of DSSCs based on

DOI: 10.1021/am507824h
ACS Appl. Mater. Interfaces 2015, 7, 2760−2771

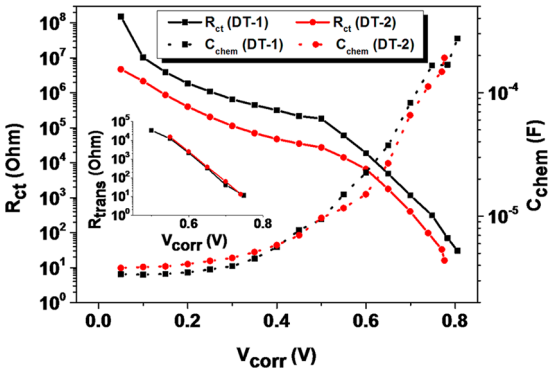

Figure 8. Charge transfer resistance (R_{ct}) and chemical capacitance (C_{chem}) of **DT-1** and **DT-2** based DSSCs extracted from the EIS measurement. Inset shows their charge transport resistance (R_{trans}). The plotted potential is corrected for the IR drop because of the series resistance.

DT-1 and **DT-2** are close to each other, indicating a very small difference between the two dyes in the energy levels of TiO_2 conduction band edge (E_{cb}).

Calculated by the equations of $\tau_n = R_{ct} \times C_{chem}$ and $\tau_{trans} = R_{trans} \times C_{chem}$,[60−62] the electron lifetime (τ_n) and electron transport time (τ_{trans}) of DSSCs based on **DT-1** and **DT-2** as the function of C_{chem} are exhibited in Figure 9. Inset shows

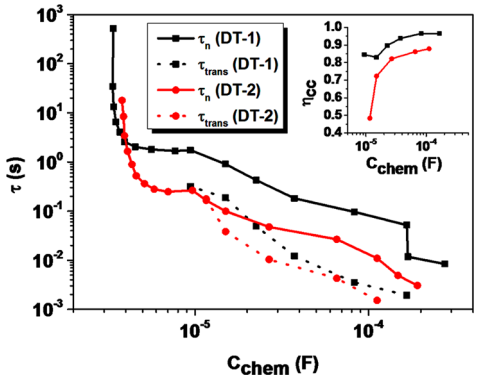

Figure 9. Electron lifetime (τ_n) and electron transport time (τ_{trans}) of DSSCs based on **DT-1** (black) and **DT-2** (red) as the function of chemical capacitance (C_{chem}) during the EIS measurement. Inset shows their charge collection efficiency (η_{cc}).

their charge collection efficiency (η_{cc}), which was obtained via the formula of $\eta_{cc} = 1/(1 + \tau_{trans}/\tau_n)$. Compared to **DT-2**, DSSC based on **DT-1** possesses much longer electron lifetime, which indicates much less charge recombination, leading to higher V_{oc}. Meanwhile, the higher η_{cc} values of DSSCs based on **DT-1** compared to **DT-2** are in good agreement with their IPCE spectra and J_{sc} values.

Above all, the results of EIS measurements show that DSSC based on **DT-1** can retard the charge recombination more efficiently than its counterpart of **DT-2** and provide some explanations for its higher V_{oc} and J_{sc}. The bigger donor size and the insulating blocking branch in the donor of **DT-1** can account for the slower charge recombination rate.

Intensity-Modulated Photovoltage Spectroscopy (IMVS). Intensity-modulated photovoltage spectroscopy (IMVS) was employed to further study recombination kinetics in DSSCs based **DT-1** and **DT-2**. Unlike EIS in the dark, IMVS was performed under incident light intensity at a certain wavelength (460 nm in our study) under open circuit conditions, which resembles better the real DSSCs working situation under illumination.[65−68] The Nyquist plots were measured under different incident light intensities. The effective electron lifetimes (τ_n) were calculated by equation of $\tau_n = 1/(2\pi f)$, in which f represents the frequency at the minimum of the semicircle plot. Figure 10 illustrates the relationship

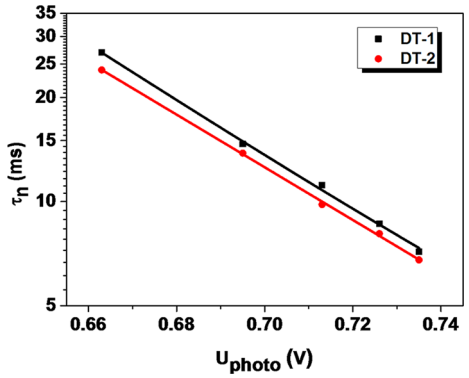

Figure 10. Electron lifetime as a function of photogenerated voltage for DSSCs based on **DT-1** and **DT-2** with cobalt electrolyte obtained by IMVS.

between the electron lifetime and the photogenerated voltage (U_{photo}). The electron lifetimes of DSSCs based on **DT-1** are slightly longer than their counterparts of **DT-2**, which further confirm that the charge recombination in DSSCs based on **DT-1** is slightly more severe than that of **DT-2**. The results show a good agreement with those extracted from EIS measurement.

CONCLUSION

In this work, two new pyrido[3,4-*b*]pyrazine-based sensitizers (**DT-1** and **DT-2**) were designed and synthesized for dye-sensitized solar cells with cobalt electrolytes and studied to understand the structure−property relationship between two different cores of bulky donor parts. The introduction of the strongly electron-withdrawing pyrido[3,4-*b*]pyrazine-based auxiliary acceptor was shown to have an effect of extending the absorption wavelength range and increasing the short-circuit current density of DSSCs compared to dye **YA422**, whose photovoltaic conversion efficiency in DSSCs has reached 10.65% but the absorption onset was only around 670 nm. An interesting circumstance about **DT-1** is that the biphenyl branch at the *cis*-position of the *N*-phenylindoline segment contributes little to the highest occupied molecular orbital (HOMO) of **DT-1**, and acts like an insulating blocking group according to density function theory calculations. However, the HOMO level of **DT-1** is less positive than that of **DT-2** due to the stronger electron donating ability of indoline than that of triphenylamine. For the device performance, the higher photoelectric conversion efficiency of 8.57% was obtained by DSSCs based on **DT-1** with cobalt redox electrolyte under standard AM 1.5 G simulated sunlight, with J_{sc} = 16.08 mA cm^{-2}, V_{oc} = 802 mV, and *FF* = 0.66. Electrochemical impedance spectroscopy (EIS) and intensity-modulated photovoltage spectroscopy (IMVS) suggest that charge recombination in DSSCs based on **DT-1** is slower than that in their counterparts of **DT-2**, owing to the larger donor size and the insulating blocking branch in the donor of **DT-1**. The longer electron lifetime of **DT-1** contributes to its higher V_{oc}; meanwhile, the

DOI: 10.1021/am507824h
ACS Appl. Mater. Interfaces 2015, 7, 2760−2771

higher charge collection efficiency also partially enhances its J_{sc}. The results indicate that indoline-based sensitizers have better performance than their triphenylamine-based analogues in DSSCs with cobalt electrolytes.

■ ASSOCIATED CONTENT

Supporting Information

The CV plots of **DT-1** and **DT-2**, the IPCE and *I*−*V* curves of DSSCs based on **DT-1** and **DT-2** with iodide electrolyte at the presence or absence of CDCA, the photovoltaic parameters of DSSCs based on **DT-1** and **DT-2** with iodide electrolyte at the presence or absence of CDCA, the simulated absorption spectra of **DT-1** and **DT-2**, the spatial distribution of LUMO + 3 of **DT-1** and LUMO + 4 of **DT-2**, computed excitation energies, oscillator strengths and molecular orbital composition for important low-lying excited states of **DT-1** and **DT-2**. This material is available free of charge via the Internet at http://pubs.acs.org.

■ AUTHOR INFORMATION

Corresponding Authors

*E-mail: ; lixin@theochem.kth.se.
*E-mail: lijhy@ecust.edu.cn.
*E-mail: jlhua@ecust.edu.cn.

Author Contributions

X.Z. and J.M. contributed equally to this work.

Notes

The authors declare no competing financial interest.

■ ACKNOWLEDGMENTS

This work was supported by the Science Fund for Creative Research Groups (21421004), the National Basic Research 973 Program (2013CB733700), and NSFC/China (21172073, 21372082, 91233207, and 21302055).

■ REFERENCES

(1) O'Regan, B.; Grätzel, M. A Low-Cost, High-Efficiency Solar Cell Based on Dye-Sensitized Colloidal TiO_2 Films. *Nature* **1991**, *353*, 737−740.

(2) Hagfeldt, A.; Boschloo, G.; Sun, L.; Kloo, L.; Pettersson, H. Dye-Sensitized Solar Cells. *Chem. Rev.* **2010**, *110*, 6595−6663.

(3) Zhang, X. L.; Huang, F.; Nattestad, A.; Wang, K.; Fu, D.; Mishra, A.; Bäuerle, P.; Bach, U.; Cheng, Y.-B. Enhanced Open-Circuit Voltage of p-Type DSC with Highly Crystalline NiO Nanoparticles. *Chem. Commun.* **2011**, *47*, 4808−4810.

(4) Hardin, B. E.; Snaith, H. J.; McGehee, M. D. The Renaissance of Dye-Sensitized Solar Cells. *Nat. Photonics* **2012**, *6*, 162−169.

(5) Grätzel, C.; Zakeeruddin, S. M. Recent Trends in Mesoscopic Solar Cells Based on Molecular and Nanopigment Light Harvesters. *Mater. Today* **2013**, *16*, 11−18.

(6) Wang, H.; Zeng, X.; Huang, Z.; Zhang, W.; Qiao, X.; Hu, B.; Zou, X.; Wang, M.; Cheng, Y.-B.; Chen, W. Boosting the Photocurrent Density of p-Type Solar Cells Based on Organometal Halide Perovskite-Sensitized Mesoporous NiO Photocathodes. *ACS Appl. Mater. Interfaces* **2014**, *6*, 12609−12617.

(7) Docampo, P.; Guldin, S.; Leijtens, T.; Noel, N. K.; Steiner, U.; Snaith, H. J. Lessons Learned: From Dye-Sensitized Solar Cells to All-Solid-State Hybrid Devices. *Adv. Mater.* **2014**, *26*, 4013−4030.

(8) Yu, Z.; Vlachopoulos, N.; Gorlov, M.; Kloo, L. Liquid Electrolytes for Dye-Sensitized Solar Cells. *Dalton Trans.* **2011**, *40*, 10289−10303.

(9) Wang, M.; Grätzel, C.; Zakeeruddin, S. M.; Grätzel, M. Recent Developments in Redox Electrolytes for Dye-Sensitized Solar Cells. *Energy Environ. Sci.* **2012**, *5*, 9394−9405.

(10) Chiba, Y.; Islam, A.; Watanabe, Y.; Komiya, R.; Koide, N.; Han, L. Dye-Sensitized Solar Cells with Conversion Efficiency of 11.1%. *Jpn. J. Appl. Phys.* **2006**, *45*, L638−L640.

(11) Komiya, R.; Fukui, A.; Murofushi, N.; Koide, N.; Yamanaka, R.; Katayama, H. Improvement of the Conversion Efficiency of A Monolithic Type Dye-Sensitized Solar Cell Module. 21st International Photovoltaic Science and Engineering Conference, Fukuoka, November, 2011.

(12) Boschloo, G.; Hagfeldt, A. Characteristics of the Iodide/Triiodide Redox Mediator in Dye-Sensitized Solar Cells. *Acc. Chem. Res.* **2009**, *42*, 1819−1826.

(13) Lu, J. F.; Bai, J.; Xu, X. B.; Li, Z. H.; Cao, K.; Cui, J.; Wang, M. K. Alternate Redox Electrolytes in Dye-Sensitized Solar Cells. *Chin. Sci. Bull.* **2012**, *57*, 4131−4142.

(14) Cong, J.; Hao, Y.; Sun, L.; Kloo, L. Two Redox Couples are Better Than One: Improved Current and Fill Factor from Cobalt-Based Electrolytes in Dye-Sensitized Solar Cells. *Adv. Energy Mater.* **2014**, *4*, No. 1301273.

(15) Cheng, M.; Yang, X.; Chen, C.; Zhao, J.; Zhang, F.; Sun, L. Dye-Sensitized Solar Cells Based on Hydroquinone/Benzoquinone as Bio-inspired Redox Couple with Different Counter Electrodes. *Phys. Chem. Chem. Phys.* **2013**, *15*, 15146−15152.

(16) Tian, H.; Gabrielsson, E.; Lohse, P. W.; Vlachopoulos, N.; Kloo, L.; Hagfeldt, A.; Sun, L. Development of An Organic Redox Couple and Organic Dyes for Aqueous Dye-Sensitized Solar Cells. *Energy Environ. Sci.* **2012**, *5*, 9752−9755.

(17) Bai, Y.; Yu, Q.; Cai, N.; Wang, Y.; Zhang, M.; Wang, P. High-Efficiency Organic Dye-Sensitized Mesoscopic Solar Cells with A Copper Redox Shuttle. *Chem. Commun.* **2011**, *47*, 4376−4378.

(18) Wang, M.; Chamberland, N.; Breau, L.; Moser, J.-E.; Humphry-Baker, R.; Marsan, B.; Zakeeruddin, S. M.; Grätzel, M. An Organic Redox Electrolyte to Rival Triiodide/Iodide in Dye-Sensitized Solar Cells. *Nat. Chem.* **2010**, *2*, 385−389.

(19) Nusbaumer, H.; Moser, J.-E.; Zakeeruddin, S. M.; Nazeeruddin, M. K.; Grätzel, M. $Co^{II}(dbbip)_2^{2+}$ Complex Rivals Tri-iodide/Iodide Redox Mediator in Dye-Sensitized Photovoltaic Cells. *J. Phys. Chem. B* **2001**, *105*, 10461−10464.

(20) Zhou, D.; Yu, Q.; Cai, N.; Bai, Y.; Wang, Y.; Wang, P. Efficient Organic Dye-Sensitized Thin-Film Solar Cells Based on the Tris(1,10-phenanthroline)cobalt(II/III) Redox Shuttle. *Energy Environ. Sci.* **2011**, *4*, 2030−2034.

(21) Yum, J.-H.; Baranoff, E.; Kessler, F.; Moehl, T.; Ahmad, S.; Bessho, T.; Marchioro, A.; Ghadiri, E.; Moser, J.-E.; Yi, C.; Nazeeruddin, M. K.; Grätzel, M. A. Cobalt Complex Redox Shuttle for Dye-Sensitized Solar Cells with High Open-Circuit Potentials. *Nat. Commun.* **2012**, *3*, 631/1−631/8.

(22) Kashif, M. K.; Axelson, J. C.; Duffy, N. W.; Forsyth, C. M.; Chang, C. J.; Long, J. R.; Spiccia, L.; Bach, U. A New Direction in Dye-Sensitized Solar Cells Redox Mediator Development: In Situ Fine-Tuning of the Cobalt(II)/(III) Redox Potential through Lewis Base Interactions. *J. Am. Chem. Soc.* **2012**, *134*, 16646−16653.

(23) Yella, A.; Lee, H.-W.; Tsao, H. N.; Yi, C.; Chandiran, A. K.; Nazeeruddin, M. K.; Diau, E. W.-G.; Yeh, C.-Y.; Zakeeruddin, S. M.; Grätzel, M. Porphyrin-Sensitized Solar Cells with Cobalt (II/III)-Based Redox Electrolyte Exceed 12% Efficiency. *Science* **2011**, *334*, 629−634.

(24) Mathew, S.; Yella, A.; Gao, P.; Humphry-Baker, R.; Curchod, B. F. E.; Ashari-Astani, N.; Tavernelli, I.; Rothlisberger, U.; Nazeeruddin, M. K.; Grätzel, M. Dye-Sensitized Solar Cells with 13% Efficiency Achieved Through the Molecular Engineering of Porphyrin Sensitizers. *Nat. Chem.* **2014**, *6*, 242−247.

(25) Tsao, H. N.; Comte, P.; Yi, C.; Grätzel, M. Avoiding Diffusion Limitations in Cobalt(III/II)-Tris(2,2′-Bipyridine)-Based Dye-Sensitized Solar Cells by Tuning the Mesoporous TiO_2 Film Properties. *ChemPhysChem* **2012**, *13*, 2976−2981.

(26) Zong, X.; Liang, M.; Fan, C.; Tang, K.; Li, G.; Sun, Z.; Xue, S. Design of Truxene-Based Organic Dyes for High-Efficiency Dye-Sensitized Solar Cells Employing Cobalt Redox Shuttle. *J. Phys. Chem. C* **2012**, *116*, 11241−11250.

DOI: 10.1021/am507824h
ACS Appl. Mater. Interfaces 2015, 7, 2760−2771

(27) Liang, M.; Chen, J. Arylamine Organic Dyes for Dye-Sensitized Solar Cells. *Chem. Soc. Rev.* **2013**, *42*, 3453−3488.
(28) Ooyama, Y.; Harima, Y. Molecular Designs and Syntheses of Organic Dyes for Dye-Sensitized Solar Cells. *Eur. J. Org. Chem.* **2009**, *18*, 2903−2934.
(29) Yum, J.-H.; Walter, P.; Huber, S.; Rentsch, D.; Geiger, T.; Nuësch, F.; Angelis, F. D.; Grätzel, M.; Nazeeruddin, M. K. Efficient Far Red Sensitization of Nanocrystalline TiO_2 Films by an Unsymmetrical Squaraine Dye. *J. Am. Chem. Soc.* **2007**, *129*, 10320−10321.
(30) Qin, C.; Wong, W.-Y.; Han, L. Squaraine Dyes for Dye-Sensitized Solar Cells: Recent Advances and Future Challenges. *Chem.—Asian J.* **2013**, *8*, 1706−1719.
(31) Nelson, J. J.; Amick, T. J.; Elliott, C. M. Mass Transport of Polypyridyl Cobalt Complexes in Dye-Sensitized Solar Cells with Mesoporous TiO_2 Photoanodes. *J. Phys. Chem. C* **2008**, *112*, 18255−18263.
(32) Klahr, B. M.; Hamann, T. W. Performance Enhancement and Limitations of Cobalt Bipyridyl Redox Shuttles in Dye-Sensitized Solar Cells. *J. Phys. Chem. C* **2009**, *113*, 14040−14045.
(33) Sapp, S. A.; Elliott, C. M.; Contado, C.; Caramori, S.; Bignozzi, C. A. Substituted Polypyridine Complexes of Cobalt(II/III) as Efficient Electron-Transfer Mediators in Dye-Sensitized Solar Cells. *J. Am. Chem. Soc.* **2002**, *124*, 11215−11222.
(34) DeVries, M. J.; Pellin, M. J.; Hupp, J. T. Dye-Sensitized Solar Cells: Driving-Force Effects on Electron Recombination Dynamics with Cobalt-Based Shuttles. *Langmuir* **2010**, *26*, 9082−9087.
(35) Feldt, S. M.; Gibson, E. A.; Gabrielsson, E.; Sun, L.; Boschloo, G.; Hagfeldt, A. Design of Organic Dyes and Cobalt Polypyridine Redox Mediators for High-Efficiency Dye-Sensitized Solar Cells. *J. Am. Chem. Soc.* **2010**, *132*, 16714−16724.
(36) Zhang, M.; Wang, Y.; Xu, M.; Ma, W.; Li, R.; Wang, P. Design of High-Efficiency Organic Dyes for Titania Solar Cells Based on the Chromophoric Core of Cyclopentadithiophene-Benzothiadiazole. *Energy Environ. Sci.* **2013**, *6*, 2944−2949.
(37) Zhang, M.; Liu, J.; Wang, Y.; Zhou, D.; Wang, P. Redox Couple Related Influences of π-Conjugation Extension in Organic Dye-Sensitized Mesoscopic Solar Cells. *Chem. Sci.* **2011**, *2*, 1401−1406.
(38) Holcombe, T. W.; Yum, J.-H.; Kim, Y.; Rakstys, K.; Grätzel, M. Diketopyrrolopyrrole-Based Sensitizers for Dye-Sensitized Solar Cell Applications: Anchor Engineering. *J. Mater. Chem. A* **2013**, *1*, 13978−13983.
(39) Xiang, W.; Gupta, A.; Kashif, M. K.; Duffy, N.; Bilic, A.; Evans, R. A.; Spiccia, L.; Bach, U. Cyanomethylbenzoic Acid: An Acceptor for Donor-π-Acceptor Chromophores Used in Dye-Sensitized Solar Cells. *ChemSusChem* **2013**, *6*, 256−260.
(40) Qin, C.; Peng, W.; Zhang, K.; Islam, A.; Han, L. A Novel Organic Sensitizer Combined with a Cobalt Complex Redox Shuttle for Dye-Sensitized Solar Cells. *Org. Lett.* **2012**, *14*, 2532−2535.
(41) Zong, X.; Liang, M.; Chen, T.; Jia, J.; Wang, L.; Sun, Z.; Xue, S. Efficient Iodine-Free Dye-Sensitized Solar Cells Employing Truxene-Based Organic Dyes. *Chem. Commun.* **2012**, *48*, 6645−6647.
(42) Li, G.; Liang, M.; Wang, H.; Sun, Z.; Wang, L.; Wang, Z.; Xue, S. Significant Enhancement of Open-Circuit Voltage in Indoline-Based Dye-Sensitized Solar Cells via Retarding Charge Recombination. *Chem. Mater.* **2013**, *25*, 1713−1722.
(43) Yang, J.; Ganesan, P.; Teuscher, J.; Moehl, T.; Kim, Y. J.; Yi, C.; Comte, P.; Pei, K.; Holcombe, T. W.; Nazeeruddin, M. K.; Hua, J.; Zakeeruddin, S. M.; Tian, H.; Grätzel, M. Influence of the Donor Size in D-π-A Organic Dyes for Dye-Sensitized Solar Cells. *J. Am. Chem. Soc.* **2014**, *136*, 5722−5730.
(44) Tsao, H. N.; Yi, C.; Moehl, T.; Yum, J.-H.; Zakeeruddin, S. M.; Nazeeruddin, M. K.; Grätzel, M. Cyclopentadithiophene Bridged Donor-Acceptor Dyes Achieve High Power Conversion Efficiencies in Dye-Sensitized Solar Cells Based on the *tris*-Cobalt Bipyridine Redox Couple. *ChemSusChem* **2011**, *4*, 591−594.
(45) Gao, P.; Kim, Y. J.; Yum, J.-H.; Holcombe, T. W.; Nazeeruddin, M. K.; Grätzel, M. Facile Synthesis of A Bulky BPTPA Donor Group Suitable for Cobalt Electrolyte Based Dye Sensitized Solar Cells. *J. Mater. Chem. A* **2013**, *1*, 5535−5544.
(46) Gabrielsson, E.; Ellis, H.; Feldt, S.; Tian, H.; Boschloo, G.; Hagfeldt, A.; Sun, L. Convergent/Divergent Synthesis of a Linker-Varied Series of Dyes for Dye-Sensitized Solar Cells Based on the D35 Donor. *Adv. Energy Mater.* **2013**, *12*, 1647−1656.
(47) Yum, J.-H.; Holcombe, T. W.; Kim, Y.; Rakstys, K.; Moehl, T.; Teuscher, J.; Delcamp, J. H.; Nazeeruddin, M. K.; Grätzel, M. Blue-Coloured Highly Efficient Dye-Sensitized Solar Cells by Implementing the Diketopyrrolopyrrole Chromophore. *Sci. Rep.* **2013**, *3*, 2446/1−2446/8.
(48) Ying, W.; Yang, J.; Wielopolski, M.; Moehl, T.; Moser, J.-E.; Comte, P.; Hua, J.; Zakeeruddin, S. M.; Tian, H.; Grätzel, M. New Pyrido[3,4-*b*]pyrazine-Based Sensitizers for Efficient and Stable Dye-Sensitized Solar Cells. *Chem. Sci.* **2014**, *5*, 206−214.
(49) Qu, S.; Qin, C.; Islam, A.; Wu, Y.; Zhu, W.; Hua, J.; Tian, H.; Han, L. A Novel D-A-π-A Organic Sensitizer Containing a Diketopyrrolopyrrole Unit with A Branched Alkyl Chain for Highly Efficient and Stable Dye-Sensitized Solar Cells. *Chem. Commun.* **2012**, *48*, 6972−6974.
(50) Wang, Z.-S.; Cui, Y.; Dan-oh, Y.; Kasada, C.; Shinpo, A.; Hara, K. Thiophene-Functionalized Coumarin Dye for Efficient Dye-Sensitized Solar Cells: Electron Lifetime Improved by Coadsorption of Deoxycholic Acid. *J. Phys. Chem. C* **2007**, *111*, 7224−7230.
(51) Becke, A. D. Density-Functional Thermochemistry. III. The Role of Exact Exchange. *J. Chem. Phys.* **1993**, *98*, 5648−5652.
(52) Lee, C.; Yang, W.; Parr, R. G. Development of the Colle−Salvetti Correlation-Energy Formula into a Functional of the Electron Density. *Phys. Rev. B* **1988**, *37*, 785−789.
(53) Hehre, W. J.; Ditchfield, R.; Pople, J. A. Self-Consistent Molecular Orbital Methods. XII. Further Extensions of Gaussian-Type Basis Sets for Use in Molecular Orbital Studies of Organic Molecules. *J. Chem. Phys.* **1972**, *56*, 2257−2261.
(54) Yanai, T.; Tew, D.; Handy, N. A New Hybrid Exchange-Correlation Functional Using the Coulomb-Attenuating Method (CAM-B3LYP). *Chem. Phys. Lett.* **2004**, *393*, 51−57.
(55) Schäfer, A.; Huber, C.; Ahlrichs, R. Fully Optimized Contracted Gaussian Basis Sets of Triple Zeta Valence Quality for Atoms Li to Kr. *J. Chem. Phys.* **1994**, *100*, 5829−5835.
(56) Frisch, M. J.; Trucks, G. W.; Schlegel, H. B.; Scuseria, G. E.; Robb, M. A.; Cheeseman, J. R.; Scalmani, G.; Barone, V.; Mennucci, B.; Petersson, G. A.; Nakatsuji, H.; Caricato, M.; Li, X.; Hratchian, H. P.; Izmaylov, A. F.; Bloino, J.; Zheng, G.; Sonnenberg, J. L.; Hada, M.; Ehara, M.; Toyota, K.; Fukuda, R.; Hasegawa, J.; Ishida, M.; Nakajima, T.; Honda, Y.; Kitao, O.; Nakai, H.; Vreven, T.; Montgomery, J. A., Jr.; Peralta, J. E.; Ogliaro, F.; Bearpark, M.; Heyd, J. J.; Brothers, E.; Kudin, K. N.; Staroverov, V. N.; Kobayashi, R.; Normand, J.; Raghavachari, K.; Rendell, A.; Burant, J. C.; Iyengar, S. S.; Tomasi, J.; Cossi, M.; Rega, N.; Millam, J. M.; Klene, M.; Knox, J. E.; Cross, J. B.; Bakken, V.; Adamo, C.; Jaramillo, J.; Gomperts, R.; Stratmann, R. E.; Yazyev, O.; Austin, A. J.; Cammi, R.; Pomelli, C.; Ochterski, J. W.; Martin, R. L.; Morokuma, K.; Zakrzewski, V. G.; Voth, G. A.; Salvador, P.; Dannenberg, J. J.; Dapprich, S.; Daniels, A. D.; Farkas, Ö.; Foresman, J. B.; Ortiz, J. V.; Cioslowski, J.; Fox, D. J. *Gaussian 09*, revision D.01; Gaussian, Inc.: Wallingford CT, 2009.
(57) Marzari, G.; Durantini, J.; Minudri, D.; Gervaldo, M.; Otero, L.; Fungo, F.; Pozzi, G.; Cavazzini, M.; Orlandi, S.; Quici, S. Fluorous Molecules for Dye-Sensitized Solar Cells: Synthesis and Characterization of Fluorene-Bridged Donor/Acceptor Dyes with Bulky Perfluoroalkoxy Substituents. *J. Phys. Chem. C* **2012**, *116*, 21190−21200.
(58) Wang, Q.; Moser, J.-E.; Grätzel, M. Electrochemical Impedance Spectroscopic Analysis of Dye-Sensitized Solar Cells. *J. Phys. Chem. B* **2005**, *109*, 14945−14953.
(59) Han, L.; Koide, N.; Chiba, Y.; Mitate, T. Modeling of An Equivalent Circuit for Dye-Sensitized Solar Cells. *Appl. Phys. Lett.* **2004**, *84*, 2433−2435.
(60) Wang, M.; Chen, P.; Humphry-Baker, R.; Zakeeruddin, S. M.; Grätzel, M. The Influence of Charge Transport and Recombination on

DOI: 10.1021/am507824h
ACS Appl. Mater. Interfaces 2015, 7, 2760−2771

the Performance of Dye-Sensitized Solar Cells. *ChemPhysChem* **2009**, *10*, 290−299.
(61) Fabregat-Santiago, F.; Bisquert, J.; Garcia-Belmonte, G.; Boschloo, G.; Hagfeldt, A. Influence of Electrolyte in Transport and Recombination in Dye-Sensitized Solar Cells Studied by Impedance Spectroscopy. *Sol. Energy Mater. Sol. Cells* **2005**, *87*, 117−131.
(62) Fabregat-Santiago, F.; Garcia-Belmonte, G.; Mora-Sero, I.; Bisquert, J. Characterization of Nanostructured Hybrid and Organic Solar Cells by Impedance Spectroscopy. *Phys. Chem. Chem. Phys.* **2011**, *13*, 9083−9118.
(63) Bisquert, J.; Mora-Sero, I.; Fabregat-Santiago, F. Diffusion-Recombination Impedance Model for Solar Cells with Disorder and Nonlinear Recombination. *ChemElectroChem.* **2014**, *1*, 289−296.
(64) Mao, J.; Yang, J.; Teuscher, J.; Moehl, T.; Yi, C.; Humphry-Baker, R.; Comte, P.; Grätzel, C.; Hua, J.; Zakeeruddin, S. M.; Tian, H.; Grätzel, M. Thiadiazolo[3,4-*c*]pyridine Acceptor Based Blue Sensitizers for High Efficiency Dye-Sensitized Solar Cells. *J. Phys. Chem. C* **2014**, *118*, 17090−17099.
(65) Zaban, A.; Greenshtein, M.; Bisquert, J. Determination of the Electron Lifetime in Nanocrystalline Dye Solar Cells by Open-Circuit Voltage Decay Measurements. *ChemPhysChem* **2003**, *4*, 859−864.
(66) Schlichthörl, G.; Huang, S. Y.; Sprague, J.; Frank, A. J. Band Edge Movement and Recombination Kinetics in Dye-Sensitized Nanocrystalline TiO_2 Solar Cells: A Study by Intensity Modulated Photovoltage Spectroscopy. *J. Phys. Chem. B* **1997**, *101*, 8141−8155.
(67) Krüger, J.; Plass, R.; Grätzel, M.; Cameron, P. J.; Peter, L. M. Charge Transport and Back Reaction in Solid-State Dye-Sensitized Solar Cells: A Study Using Intensity-Modulated Photovoltage and Photocurrent Spectroscopy. *J. Phys. Chem. B* **2003**, *107*, 7536−7539.
(68) Van de Lagemaat, J.; Park, N. G.; Frank, A. J. Influence of Electrical Potential Distribution, Charge Transport, and Recombination on the Photopotential and Photocurrent Conversion Efficiency of Dye-Sensitized Nanocrystalline TiO_2 Solar Cells: A Study by Electrical Impedance and Optical Modulation Techniques. *J. Phys. Chem. B* **2000**, *104*, 2044−2052.

DOI: 10.1021/am507824h
ACS Appl. Mater. Interfaces 2015, 7, 2760−2771